Transport Phenomena in Micro- and Zero-Gravitational Fields [1]

Johannes Straub

LATTUM, Technical University of Munich, Arcisstr. 21, D–8000 Munich 2, Germany

Abstract

The knowledge and the prediction of the transport phenomena in a micro-gravity environment are of essential importance for their application in space and for basic studies of convective heat and mass transfer without forced convection and buoyancy as driving force. There are contrary demands. In materials processing, heat conduction and mass diffusion are the only transport mechanisms desired to achieve high-quality materials, therefore convection should be avoided. In contrast, for heating and cooling applications, enhanced heat transfer by convection and two-phase transport mechanisms is highly desirable in order to minimize the occurring temperature differences and the necessary area in heat exchangers. Therefore, we discuss in this paper the influence of acceleration disturbances on the onset of convection, furthermore, the enhancement of heat and mass transfer by thermocapillary flow, which occurs, when a free surface is present. Finally, results of boiling heat transfer in micro-gravity are presented as examples for two-phase systems.

Introduction

Nowadays, great efforts are made to study transport phenomena without the effects caused by earth-gravity. If pressure-driven forced convection can be excluded in a micro-gravity environment, the question arises, what are the remaining convective transport mechanisms for heat and mass transfer, besides pure conduction and diffusion. One the one hand, in material processing convective processes should be avoided, because it is generally assumed that the quality of the material is improved enormously, if the solidification process is governed by pure conduction and diffusion only. The problem arises by the fact that all materials are processed out of, either a liquid or a gaseous phase thus inhomogenities or striations in the material are caused by transient convection, which is connected with a transient

mass transfer to the solidification front. Such convection is induced by acceleration disturbances or by thermocapillary flow, which can easily lead to oscillatory convection due to a superposition of various mechanisms. On the other hand, there are applications even in space vehicles, where convective heat and mass transport is necessary for heating and cooling devices and for energy conversion. In this case, the question is, which system can provide high heat transfer rate. Furthermore, studies on transport phenomena are of general and fundamental nature for the basic understanding of the driving mechanisms themselves, when buoyancy is excluded.

Thus, the question of transport phenomena in micro-gravity is a major one to understand materials processing and fluid behavior for both space and earth applications. In the following report, some examples and results of our research are discussed, such as:

- convection induced by acceleration disturbances;

- convection induced by thermocapillarity, and the corresponding enhancement of heat transfer;

- heat transport with phase change in two-phase systems, like boiling.

To avoid misunderstanding, we first clarify the term micro-gravity. Strictly speaking, there exists no micro- or zero-gravitational field. One can achieve a micro-gravity environment by compensation of earth-gravity, either by acceleration or deceleration or by a centrifugal force acting in such a way that the forces on the body compensate each other according to the fundamental laws of mechanics. The first one can be realized in free-fall systems, like drop towers, ballistic rocket and aircraft flights, the second one in orbital systems.

Convection Induced by Acceleration Disturbances

Since materials science experiments have been performed in a micro-gravity environment, a lively discussion about the influence of acceleration disturbances on material samples has come up and is still going on. Such interferences of the

micro-gravity level induce convection in liquids, when they are differentially heated in their process containers. This unsteady convection causes unsteady mass transfer and, in turn, inhomogeneities in the solid material or in the crystal structure, if such perturbations occur during the solidification process. On earth, such disturbances cannot be studied experimentally. Therefore the onset of convection and the development of the transient flow field under acceleration disturbances is examined by numerical simulations [1]-[5].

1 Magnitude of Disturbances

In an orbital system, both external and internal forces may give rise to acceleration disturbances. External forces are caused by operational activities, such as thruster firings for position control. The main direction of such disturbances is along the axis of the orbiter vehicle with highest spikes of $6 \cdot 10^{-2}g$. Internal forces result from mass allocation inside the space vehicle due to mechanical motions of experimental facilities and crew activities. Impulses caused by them are always compensated by negative impulses of the same size delayed in time corresponding to the resonant frequency of the experimental module overlapped by the natural frequency of the spacelab module in its suspension. Typical spikes have amplitudes of less than $10^{-2}g$, but often they are random in their direction. In quiet phases, peaks of the resulting gravity vector are recorded to be $2 \cdot 10^{-4}g$ in maximum. Considering these facts, it is obvious that a general prediction of the influence of gravity disturbances cannot be given. Firstly, they depend on the space vehicle and the mission itself; most of the disturbances are random in direction, amplitude, and time of their occurring. Secondly, the experiment itself, the geometry, the size of the temperature gradient in the liquid, the direction of the acceleration vector with respect to the temperature gradient, and the properties of the fluid are of considerable importance.

2 Numerical Model

The problem under consideration is sketched in Fig. 1. The transient 3-dimensional buoyancy-driven flow in a cylindrical enclosure filled with fluid is governed by the well-known conservation equations for mass, momentum, and energy. At all rigid walls, we assume non-slip conditions. The thermal boundary conditions are isothermal top and bottom walls. Furthermore, a perfectly insulated lateral wall is assumed (Fig. 1). For gases, the equation of state for an ideal gas applies, while the density of liquids depends linearly on the temperature. The aspect ratio of height H to diameter D is defined as $A = H/D$. The inclination angle α of the cylinder's axis towards the direction of the gravity field, the Prandtl and Rayleigh numbers can be varied independently. The acceleration pulse amplitude is given by a modified Rayleigh number Ra^*, with g^* as the acceleration:

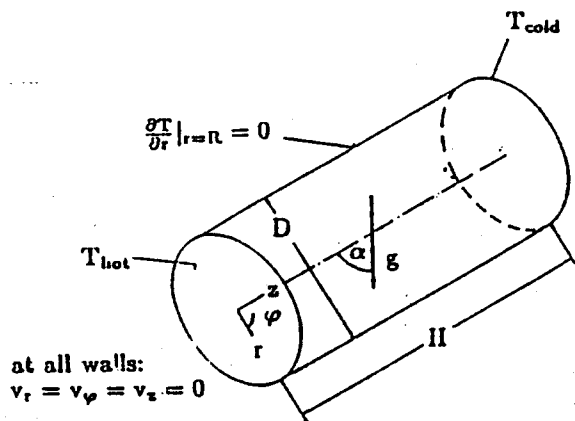$$Ra^* = \frac{g^* \beta_p D^3 (T_{hot} - T_{cold})}{\nu a} \qquad (1)$$

Figure 1: Scheme of the cylinder with boundary conditions and gravity vector.

A modified Fourier number Fo^* describes the pulse duration $\hat{t}$ or oscillation period:

$$Fo^* = \frac{\hat{t} a}{D^2} \qquad (2)$$

The transient flow field is fully calculated, and the maximum velocity is determined in order to describe the intensity of the fluid motion. Even if location and direction of the maximum velocity vary, its magnitude is an upper limit for all occurring velocities in the fluid, and it is used in the graphs to characterize the intensity of the flow. The dimensionless velocity v^* is defined as:

$$v^* = \frac{vD}{a} \qquad (3)$$

For a series of impulses, we use the dimensionless frequency:

$$f^* = \frac{fD^2}{a} = \frac{1}{Fo^*} \qquad (4)$$

Table 1: Properties of the investigated fluids

fluid	Pr	ν	a	ϱ_0	T_0	β_p
	[−]	$[10^{-6}\frac{m^2}{s}]$	$[10^{-6}\frac{m^2}{s}]$	$[\frac{kg}{m^3}]$	[K]	$[10^{-4}\frac{1}{K}]$
silicon	0.023	0.3	13.0	2500	1690	1.43
air	0.71	15.1	21.3	1.2045	293	34.13
water	7.0	1.0	0.14	998.2	293	1.8
glycerin	134.9	11.9	0.088	1260.4	293	4.9

To investigate the influence of the properties, four different fluids are used for the calculation: silicon, air, water, and glycerin (Tab. 1). In thermofluid-dynamic problems, the Prandtl number is an important property, which is varied with the selected fluids over about four decades from 10^{-2} to 10^2. For the low Prandtl number fluid silicon, the calculation consumes much more CPU time than for the other fluids.

3 Results

Onset of Convection

The angle α between the temperature gradient and the vector of acceleration is important for the onset of convection. If the acceleration vector is in opposite direction to the temperature gradient, the density stratification is stable ($\alpha = 180°$, Fig. 1), and heat is transferred by conduction only. For $\alpha = 0°$, the acceleration vector and the temperature gradient act in the same direction, this configuration is metastable, the onset of convection depends on the Ra number and the aspect ratio. This case is well-known as Rayleigh-Bénard problem. The critical Rayleigh number obtained by our numerical calculations is in good agreement with experimental and theoretical results from other authors, and can be regarded as a test for the numerical code (Fig. 2) [5].
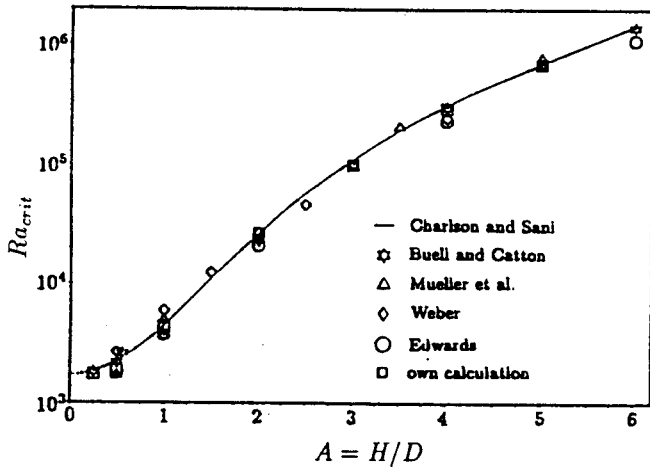

Figure 2: Onset of convection and critical Ra number for the Rayleigh-Bénard problem dependent on the aspect ratio of the cylinder.

For all other orientations of the acceleration vector $0° < \alpha < 180°$, the density stratification is unstable. For the case of an axial linear temperature profile between top and bottom, the convection sets in immediately after an acceleration pulse.

In Figs. 3 and 4, the transient development of the maximum dimensionless velocity v^*_{max} and the Nu number are shown, after a gravity pulse from initially $Ra = 0$ at $Fo = 0$ to $Ra^* = \text{const.}$ for $Fo > 0$ has been exerted. For small angels of $\alpha \approx 1°$, a slow fluid reaction is observed. Steady-state conditions are achieved for $Fo > 0.5$, and for larger angles for $Fo < 0.1$.

Single Rectangular Pulse

The effect of external forces caused by thruster firings for position control of the orbiter is simulated by single rectangular pulses. Pulses of different amplitudes Ra^* and durations Fo^* are applied perpendicularly ($\alpha = 90°$) to the
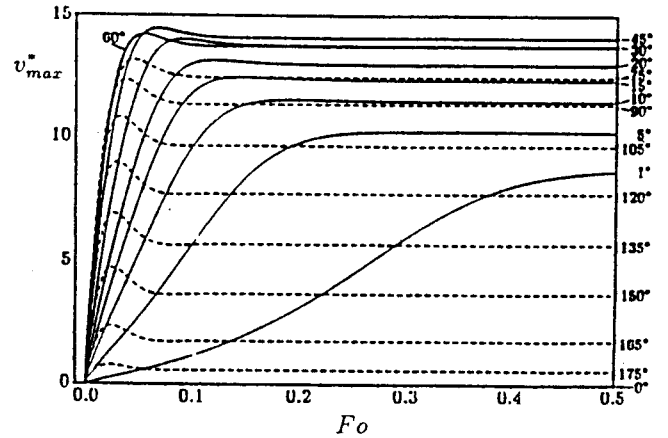

Figure 3: Development of the flow field v^*_{max} with Fo after a acceleration step pulse.
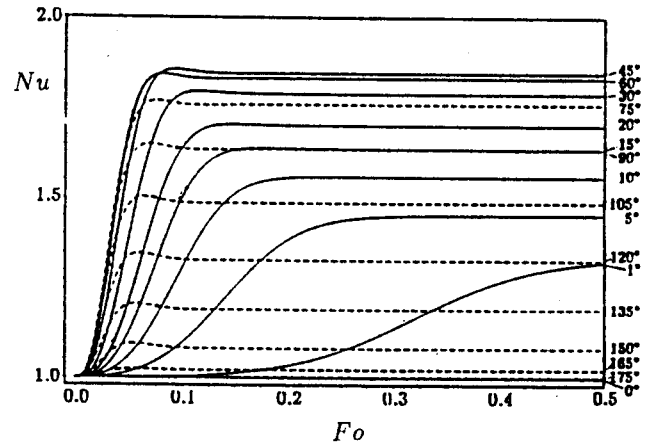

Figure 4: Averaged Nusselt number Nu with time Fo. The fluid is air, $Ra^* = 5000$.

temperature gradient. If Fo^* exceeds 0.1, steady-state conditions with a constant velocity and Nu number are achieved. The initial conditions are, as mentioned above, no motion due to low-gravity and linear temperature profile between the differentially heated end walls. For the same pulse duration Fo^*, the maximum peak velocity at the end of the pulse is directly proportional to the amplitude of the pulse, where C is constant for a certain aspect ratio:

$$v^*_{max,peak} = C \cdot Ra^* \qquad (5)$$

Thus, all graphs of Fig. 5 coincide on one curve, if the ratio of $v^*_{max,peak}/Ra^*$ is used for the ordinate. The convective flow fades away exponentially, after the pulse has been applied:

$$\frac{v^*_{max}}{v^*_{max,peak}} = \exp\left(\frac{Fo^* - Fo}{\tau}\right) \qquad \text{for} \quad Fo > Fo^* \quad (6)$$

Table 2: Decay constant τ of the flow in Eq. (6)

A	0.5	1.0	2.0	5.0
τ	0.020	0.038	0.053	0.061

The decay constant τ depends on the aspect ratio A (Table 2). Fig. 5 is calculated for air; a general transformation to the other fluids seems possible, if the transient flow Fourier number $\widetilde{Fo} = Fo \cdot Pr$ is used.
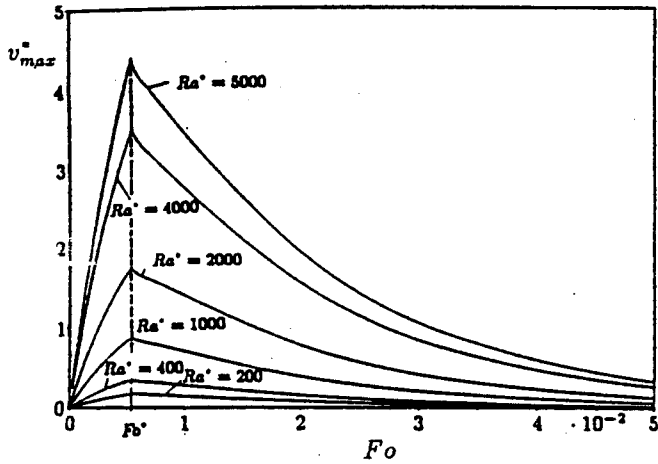

Figure 5: Maximum velocity v^*_{max} versus dimensionless time Fo for rectangular pulses of different amplitude Ra^*.

Periodic Pulses

Periodic pulses with alternating acceleration vectors are caused by internal forces from mass allocation inside the space vehicle. They may be simulated by sinusoidal or rectangular periodical pulses.

The maximum velocity is nearly independent of the form of the pulses, however, as discussed before, for low frequencies ($f^*/Pr < 10$) it depends on the acceleration amplitude, and steady-state conditions are obtained after each reversal of the acceleration pulse. At a cut-off frequency of $f^*/Pr = 10$, the velocities decrease, because the flow is just opposite to the direction of the excited new pulse. The inertia of the flow must first be overcome, before the flow turns around and follows the direction of the new pulse. If the maximum velocity is plotted versus the dimensionless frequency (Fig. 6),

$$\frac{f^*}{Pr} = f \cdot \frac{D^2}{\nu} = \frac{1}{Fo^* \cdot Pr} \qquad (7)$$

the decay of the maximum velocity coincides on one curve for the various fluids. The system is dominated by the kinematic viscosity ν rather than by the thermal diffusivity a.

Although these results are strictly valid only in the range of the investigated parameters, more general conclusions, how convection in a micro-gravity environment caused by acceleration perturbations can be avoided, are possible:

- Accelerations perpendicular to the temperature gradient induce greater velocities than those in parallel direction, and the reaction is much faster.
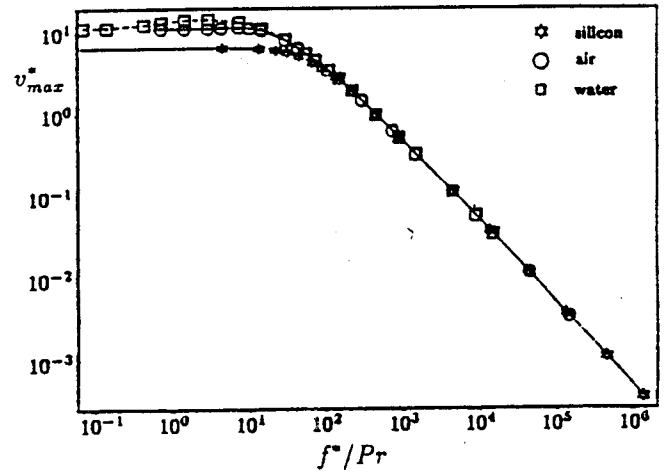

Figure 6: Maximum velocity for various fluids for periodical pulses of $Ra^* = 5000$ with frequency $f^*/Pr = f \frac{D^2}{\nu}$ as time scale.

- The effects of residual acceleration can be reduced, if the experimental set-up is aligned in such a manner that the acceleration vector acts in opposite direction of the temperature gradient.

- The maximum velocities are proportional to the acceleration amplitude Ra^*, i.e. the velocities increase for a given acceleration with the third power of the dimension in the direction of the acceleration vector.

- Disturbances of high frequency are less significant than those of low frequency.

- A periodical series of positive and negative accelerations induce lower velocities than a single pulse of the same duration for $f^*/Pr > 10$.

It is obvious that only general statements and recommendations for planning space experiments can be derived from these results. For very sensitive experiments, special 3-dimensional calculations have to be performed, where all parameters of influence can be considered.

Thermocapillary Convection

When a liquid-liquid or a liquid-gas interface is exposed to a temperature or concentration gradient, a flow termed Marangoni, surface tension-driven convection or, in the case of a temperature gradient, thermocapillary convection is induced in the liquid in direction of higher surface tension. In most fluids, surface tension decreases with increasing temperature, thus, a convective flow is induced from higher to lower temperature thus supporting the heat transfer. Due to the dominance of buoyancy over thermocapillary convection on earth, this form of natural convection was not paid much attention to for a long time. In addition, it is impossible to separate the effects evoked simultaneously

by both buoyancy and surface tension convection in experiments on earth. However, with the technical feasibility of experiments on board of orbiting spacecrafts, on ballistic rockets or in drop towers, an increasing interest has been directed towards the research of Marangoni flows. Under micro-gravity, containerless processing methods, such as floating zone melting and solidification, and Czochralski crystal growth have been focused on. Any kind of convection is undesired in those processes. Buoyancy convection can be suppressed, while Marangoni convection can hardly be avoided in case of a free surface subjected to a temperature gradient. From the viewpoint of heat and mass transport, however, thermocapillary convection enhances the heat transferred through the liquid. Three examples are discussed in the following.

1 Experimental Studies

To demonstrate the effect of thermocapillary flow, the heat transfer around a single steam bubble is studied. A plate heater is mounted upside down in subcooled R113. A single bubble is created (Fig. 7) and observed by holographic interferometry. In some distance from the bubble, the interferometer fringes show a temperature profile due to pure conduction, as the density stratification is stable, and no buoyancy convection occurs. On both sides of the bubble, strong convection is induced by thermocapillary forces and this flow is strong enough to act against the buoyancy force. The enhancement of heat transfer is investigated in various liquids by the arrangement sketched in Fig. 8 [6]. A platinum wire of 0.02 mm in diameter and 3 mm in length merged in the liquid serves both as heater and resistance thermometer. The heat flux through the wire is kept low enough so that only free convection occurs. By a special holder, a semispherical air bubble of 2.5 mm in diameter is positioned in a way that the wire is just touched by the bubble.
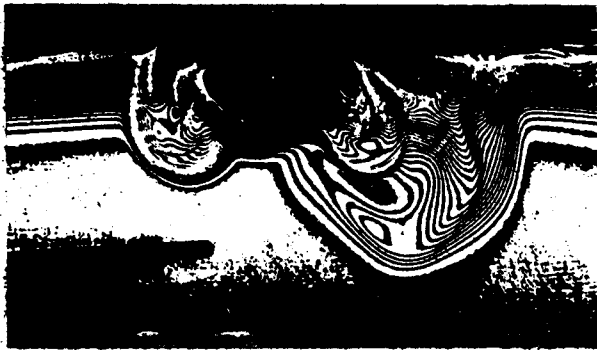

Figure 7: Thermocapillary flow in subcooled R113 observed by holographic interferometry. The bubble is in upside-down position.

The flow around the bubble is observed by tracer particles, while the heat transfer is measured by the change of the temperature and resistance of the wire, respectively. Immediately when the air bubble touches the wire surface, thermocapillary flow sets in and the wire temperature is

Figure 8: Air bubble of 2.5 mm in diameter on a heated platinum wire.

reduced. In Fig. 9, the increase of the heat transfer is represented by the Nu number as a function of the Marangoni number, which is defined as:

$$Ma = \frac{d\sigma}{dT} \cdot \frac{\Delta T D}{a\eta} \qquad (8)$$

with σ as the surface tension, D the diameter of the wire, a the thermal diffusivity, η the dynamic viscosity, and ΔT the temperature difference between the wire and the bulk liquid.
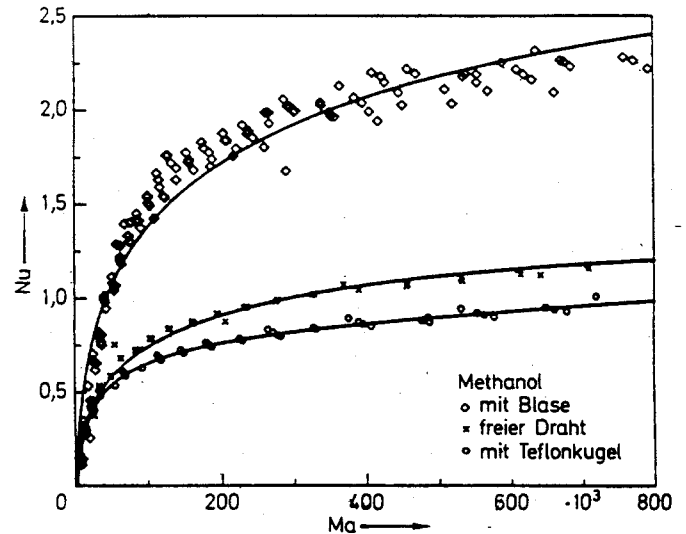

Figure 9: Enhancement of heat transfer by thermocapillary flow on a wire submerged in methanol.

To prove that the enhanced heat transfer is due to Marangoni convection, a solid Teflon sphere of diameter D is brought in the same position on the wire. As expected, the heat transfer is reduced because of the obstacle to the flow. This is a clear evidence that thermocapillary flow contributes to heat transport very efficiently.

For this experiment we used various liquids, like methanol, propanol, ethanol, R113, water, and mixtures of water and methanol. In case of pure water, it should be mentioned that Marangoni convection could not be observed for a longer period. Contrary, a mixture of 20 % methanol and 80 % water exhibited the usual thermocapillary flow. The deficiency of

Marangoni convection in the case of pure water is usually explained by the contamination of the water surface. However, if this was true, the contamination should have had an effect not only on the surface tension itself, but also on the surface tension gradient and reduce this gradient to zero. It seems worth to study this effect with water in more details. As mentioned before, it is difficult to separate the effects of buoyancy and thermocapillary convection in earth experiments. Therefore, numerical simulations are decisive tools to study them. They also help to support the planning of space experiments, to facilitate the design of new equipment and to reduce the number of expensive space experiments. Two numerical examples are discussed below.

2 Numerical Studies

Transient Marangoni convection is simulated around a gas bubble floating in a rectangular cavity filled with liquid. The side walls are adiabatic, while the bottom and the top walls are maintained at different temperatures. Two 2-dimensional numerical methods are employed, a finite difference scheme with explicit time steps and a fully implicit control-volume finite element method. To simplify the calculations, the bubble is fixed in the middle of the container neglecting buoyancy effects and the force exerted on the bubble by the thermocapillary flow around it. The magnitude of this force is calculated. It can be regarded as the holding force necessary to keep the bubble in place, otherwise it would migrate in the direction of the higher temperature. Variable gravity conditions make it possible to study the interaction of buoyancy and surface tension-driven convection. The system under consideration is governed by the conservation laws for mass, momentum, and energy. As fluid properties the values of water are used, because they are easily available and for the principle study it is of secondary interest that with water thermocapillary convection can not be maintained stationary. In a first approximation, the 3-dimensional problem is reduced to 2 dimensions by considering only a cross-section of the bubble. The special combination of circular and rectangular geometry excludes the use of regular grids. Special elements are used to approach the curved surface of the bubble. For details of the numerical methods we refer to [7] and [8]. The temperature field around the bubble without buoyancy is closely connected with the flow field (Fig. 10).

When the temperature difference between bottom and top walls of the container or the Marangoni number, respectively, is increased, the heat transfer is enhanced and the isotherms accumulate near the heated and cooled walls. The number of isotherms originating from the bubble surface decreases with increasing Marangoni number. With an increasing gradient of surface tension around the bubble, two vortices develop due to the recirculating flow. In Fig. 11, the influence of earth-gravity acting in either parallel or opposite direction of the thermocapillary flow is obvious. In the case of Marangoni convection acting against buoyancy (**M−B**), the initial temperature field causes a stable vertical density stratification. The displacement of the isotherms accounts
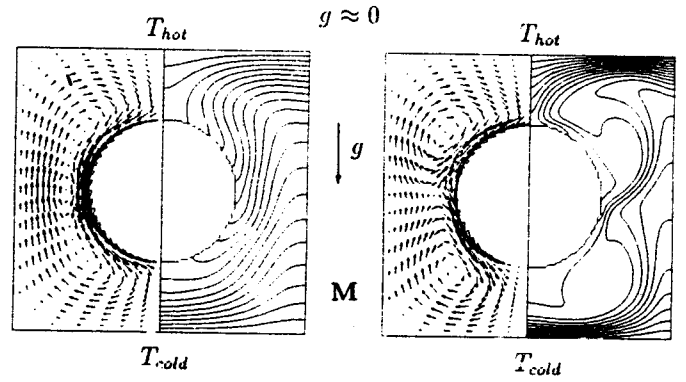

Figure 10: Predicted velocity fields (left) and isotherms (right) for increasing Marangoni numbers under micro-gravity $Ma = 5000$ (left), and $Ma = 100000$ (right).
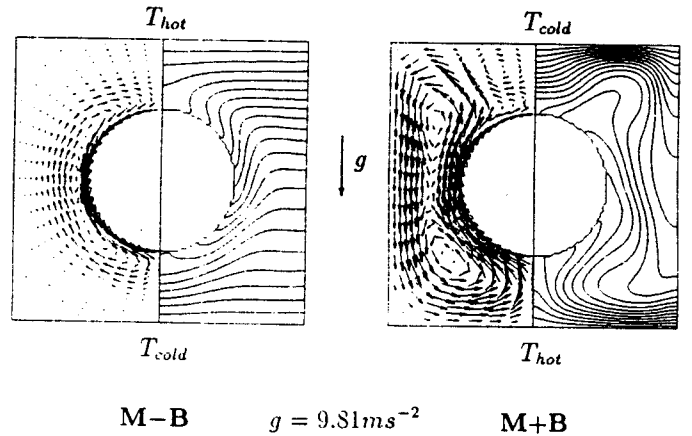

Figure 11: Interaction between thermocapillary flow and buoyancy. **M−B** ($Ma = 10000$) denotes the case of counteraction, **M+B** ($Ma = 5000$) the case of cooperation.

for the effect of the thermocapillary flow being in opposite direction of buoyancy. Compared to micro-gravity conditions, buoyancy pushes the recirculating flow closer to the bubble surface. With **M+B**, an unstable density stratification is chosen as initial condition in the cavity so that thermocapillary flow and buoyancy convection augment each other. Now, the recirculating flow is governed by one large vortex filling up the whole cavity. The influence of thermocapillary convection can be demonstrated quantitatively in the enhanced heat transfer, as in the plot of the Nu number versus the Ma number (Fig. 12).

Pure conduction inside the cavity with inactive bubble is defined as $Nu = 1$; it should be emphasized that in this case the bubble has an insulating effect, the heat transfer is 67.5 % lower as in the case of a cavity completely filled with liquid. The steady-state Nu number increases significantly, when a Marangoni number of $Ma = 10^2$ is exceeded. In a range of $1 \leq Ma \leq 10^2$, convection is still existent, however, its contribution to heat transfer can be neglected. The behavior that a certain Marangoni number is necessary
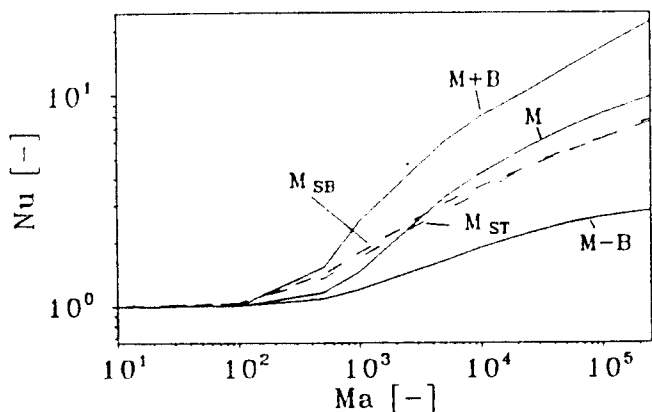
Figure 12: Heat transfer depending on the Marangoni number for the various cases investigated.

Figure 13: Oscillatory heat transfer at higher Marangoni numbers.

for an observable increase in the Nusselt number is already known from buoyancy convection. As expected, the biggest enhancement of heat transfer is the buoyancy supported thermocapillary flow (M+B) in Fig. 12. The case, where buoyancy convection acts against Marangoni flow (M−B), has the lowest increase in the Nu number. However, it must be recognized that even here the heat transfer is enlarged, i.e. the thermocapillary flow is strong enough to exceed the buoyancy flow. For pure Marangoni convection, the heat transfer is about eight times higher than for pure heat conduction at $Ma = 10^5$. In Fig. 12 the heat transfer of a semi-spherical bubble attached either to the bottom (M_{SB}) or to the top (M_{ST}) of the enclosure, is included additionally. In both cases, the heat transfer is little less than that of a spherical bubble of the same diameter. At higher Ma numbers, the strong increase of the Nu number is reduced. This is due to the reduction of the isotherms on the bubble surface.

3 Oscillatory Behavior

Within the range of $5 \cdot 10^3 < Ma < 2 \cdot 10^5$, an overshooting of the Marangoni flow at the beginning of the calculation is observed causing damped oscillations vanishing in the steady state. At higher Ma numbers, steady oscillatory flow patterns and temperature fields are maintained leading to an oscillation of the Nu numbers at top and bottom, too (Fig. 13). Various tests show that numerical influences can almost be excluded as reasons for this behavior. These oscillations can physically be explained. The strong convection at the bubble interface reduces the local temperature gradient itself and in consequence the velocity of the flow. Now, with the reduced flow, the temperature gradient at the interface recovers and strengthens the convection again. A periodic oscillation of two vortices, one in the upper, the other in the lower part of the cavity is stabilized and determines the flow and temperature fields. In case of pure Marangoni convection, the beginning of periodic oscillation is observed at $Ma \approx 250000$. This value is shifted to lower Marangoni numbers, when thermocapillary flow is supported by buoyancy.
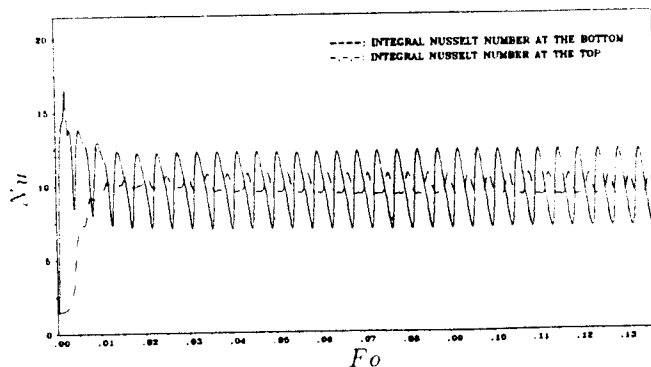
4 Liquid Column Flow

Regarding the discussion above, it is interesting to note that we could not confirm the oscillating flow in a 3-dimensional numerical simulation of a liquid column as recently described by several authors [9]–[14]. The physical mechanism of oscillatory Marangoni convection in a floating zone is discussed in [15]–[17], however, it is not completely understood yet. Further numerical studies and experimental ones by other authors on space flights are planned. The thermocapillary flow in cylindrical floating zones has been studied as a model for crystal growth configurations both numerically and experimentally under micro- and earth-gravity. The critical Marangoni number Ma_c for the onset of the oscillation is widely ranging between $100 < Ma_c < 1.6 \cdot 10^4$ in the experiments, as well as in the numerical studies. The last ones are often based on 2-dimensional calculations, while it is generally assumed that oscillations of the flow and temperature fields are of 3-dimensional nature. Therefore, we have studied this thermocapillary problem with the 3-dimensional code as mentioned above [18], [19]. In the vertical liquid column under consideration, similar to Fig. 1, top and bottom are heated and cooled, both walls are isothermal and rigid, and non-slip conditions apply. The lateral cylindrical side, however, is regarded as a non-deformable free surface subject to the Marangoni boundary conditions. The aspect ratio of the liquid bridge is $H/D = 1$, with D the diameter of the cylinder and H the height of the zone.

Pure thermocapillary convection forms a 2-dimensional axially symmetric toroidal vortex under micro-gravity ($g \rightarrow 0$), while buoyancy convection alone ($1 - g$) produces a non-symmetrical 3-dimensional single roll. Varying the gravity level in the simulation, a superposition of both kinds of convection implies 3-dimensional temperature and flow fields. Due to lack of space, only a few aspects of this study are given:

The basic flow mode is already established after a few seconds, and after 50 s steady-state flow is achieved (Fig. 14). A S-shaped temperature profile develops along the free surface (Fig. 15). Within a distance of about 10 % from the bottom and the top, the temperature gradients are significantly reduced, thus, in the center of about 80 % of the column length, only a very small gradient is in action.
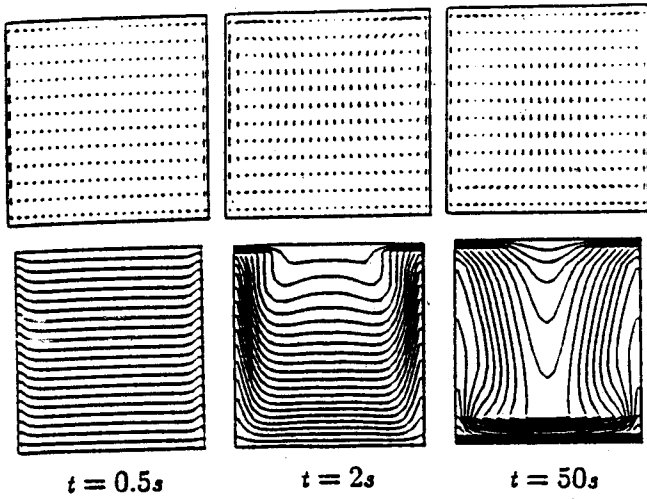
$$t = 0.5s \qquad t = 2s \qquad t = 50s$$

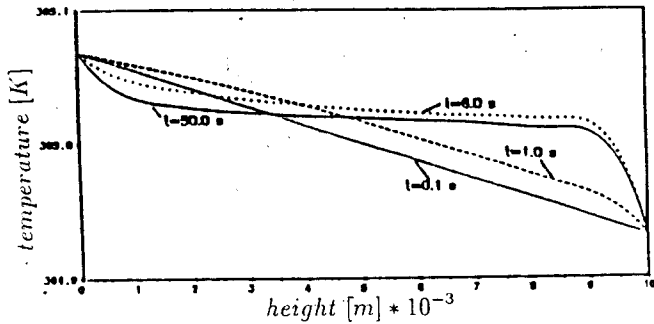Figure 14: Transient development of the flow and temperature fields in a liquid column.

Figure 15: Development of a S-shaped temperature profile along the free surface.

The overall heat transfer expressed by the integral Nu number in Fig. 16 is depicted up to $Ma = 10^7$. As discussed before, up to $Ma \approx 10^2$ there is no significant deviation of the Nusselt number from unity, which represents pure heat conduction. With higher Ma numbers, the velocities and the Nu numbers rise due to an increasing thermocapillary force. For $Ma > 10^5$, a gradual decline in heat transfer occurs as in the case of the bubbles as observed both experimentally and numerically. At $Ma = 10^7$, a saturation of the heat transfer towards a constant Nu number $Nu \approx 14$ is exhibited.

For $Ma = 5000$, the steady-state heat transfer at three different gravity levels or Bond numbers ($Bo = Ra/Ma$), respectively, is given in terms of the Nu number (Tab. 3). It is interesting to note that the heat transfer of pure buoyancy convection is only 38 % of that of thermocapillary flow. The interaction of Marangoni and buoyancy-driven convection is surprisingly weak. If both mechanisms work in same direction, the increase in the heat transfer rate is only about 7 %, when they counteract the reduction is about 9 %.
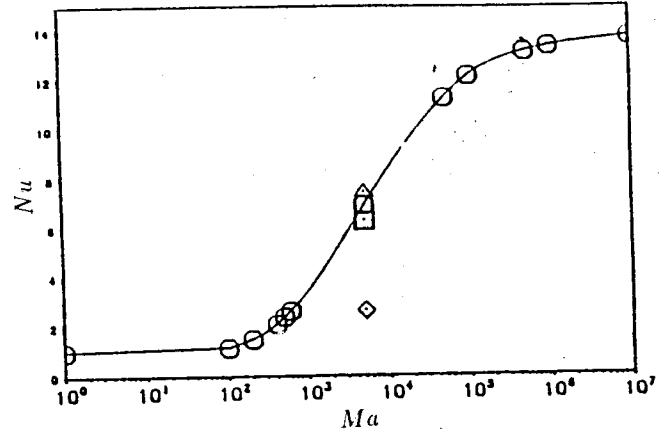

Figure 16: Nusselt number versus Marangoni number for the liquid column.

Table 3: Integral steady-state Nusselt number for different gravity levels (MC=Marangoni convection, BC=buoyancy convection)

g-level	0-g	μ-g	1-g	1-g	1-g
Remarks	pure MC	MC ⇈ BC	MC ⇈ BC	MC ⇊ BC	pure BC
Bo	3.6 E-40	3.6 E-02	3.6 E00	3.6 E00	∞
Ra	1.8 E-36	1.8 E02	1.8 E04	1.8 E04	1.8 E04
Ma	5.0 E03	5.0 E03	5.0 E03	5.0 E03	0.0 E00
Nu	6.922	6.928	7.44	6.29	2.65

Pool Boiling

As a last example for transport mechanisms under microgravity, pool boiling is discussed. Transport processes with phase change are the most efficient modes of heat transfer characterized by small temperature differences and high specific heat fluxes. Therefore, they are employed in most thermal energy conversion and transport systems, as well as in heating and cooling devices. Due to the great differences in the densities between the surrounding liquid and the vapor bubbles, it is generally assumed that the heat transport in pool boiling is highly influenced by buoyancy forces. Thus, gravity is regarded as an important factor in all physically based or empirical correlations for pool boiling heat transfer. Tests in a micro-gravity environment provide a means to study the real influence of gravity and to separate gravity-related to gravity-independent factors.

In the first stage of our experimental studies in micro-gravity, the most important question was, whether nucleate pool boiling can be maintained without buoyancy forces. Furthermore, what mechanisms are able to provide similar high heat flux rates as high as on earth, and which forces can replace the effect of gravity.

The boiling process is very complex because of the interdependence of numerous factors and effects, such as the interaction between the solid surface of the heater with the liquid and vapor, the interaction between the liquid and vapor itself, and the transport of liquid and vapor from the

heater surface. This complex behavior is the reason that – despite of nearly 6 decades of boiling research – the physics of the boiling process itself is not properly understood and is poorly represented in most correlations. This becomes evident from the fact that the usefulness of most correlations diminishes very rapidly, if they are used outside the range of the physical parameters for which they were developed [20]. Thus, a micro-gravity environment offers the unique opportunity to study these complex interaction processes without or, at least, with reduced buoyancy forces.

To answer the numerous open questions arising with boiling, we started to carry out boiling experiments in micro-gravity about 15 years ago. We used available facilities by which the earth-gravity can be compensated, such as ballistic rockets within the German TEXUS program, parabolic flights with aircrafts from NASA. Now we are preparing an experiment for the Space Shuttle scheduled on the D2-mission for January 1993. In the following, some of our recent findings are presented. For more details see [21]–[24].

1 Nucleate Boiling

Saturated and subcooled pool boiling have been investigated in parabolic aircraft flights. The fluid used is R12, the pressure ranges from $0.1 < p/p_c < 0.7$, with p_c the critical pressure. Platinum wires of 0.2 and 0.05 mm diameter, a gold-coated tube of 8 mm diameter, and a gold-coated plate of 40 mm × 20 mm are used as heaters. The platinum wire and the gold coating served as heaters and resistance thermometers simultaneously to determine the surface temperature of the heater. A typical parabola sequence of saturated nucleate boiling is shown in Fig. 17 using a 0.2 mm-wire at a pressure of $p/p_c = 0.18$. The gravity level a/g, the temperature difference $\Delta T_{sat} = T_w - T_{sat}$, and the power q_w supplied to the heater are plotted versus the experimental time. The power was switched on during the low-gravity period, at 40 s on the time scale, eliminating thus convection before the microgravity state was reached. Due to the small heat capacity of the wire, the temperature responded immediately after the power was turned on. At 45 s, the power was increased stepwise, the wire temperature reacted without delay. The
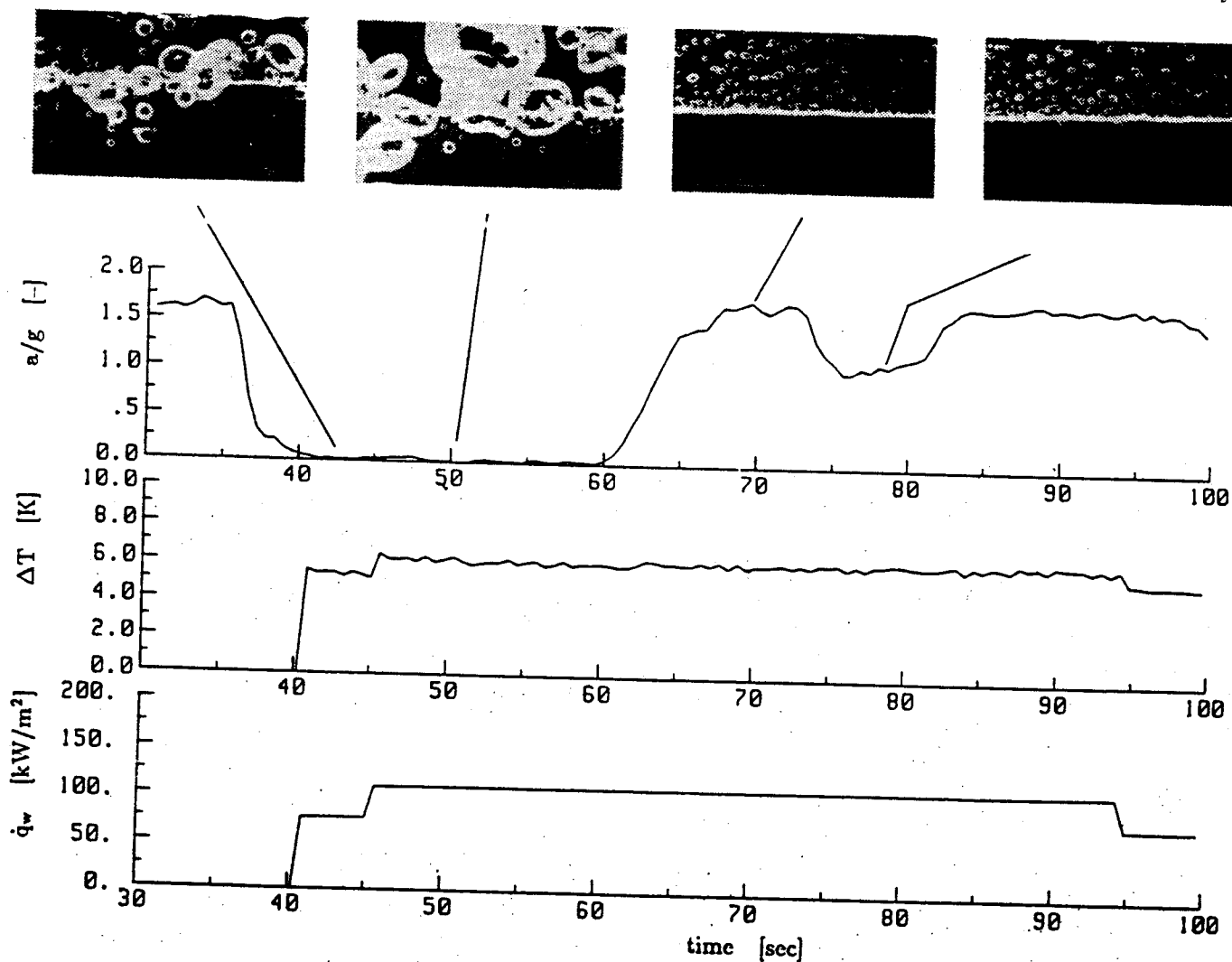

Figure 17: A parabola sequence with photographs of bubbles, the acceleration level, the wire temperature, and the heat flux during nucleate boiling for $p/p_c = 0.18$.

duration of the low-gravity period was about 20 s. After that, the acceleration increased from about $a/g \approx 0.01$ to 1.8, and decreased to earth-gravity $a/g = 1$. Thus, in one parabola sequence the boiling behavior at micro-gravity and at higher accelerations could be studied. The low-gravity period of 20 s was long enough to achieve steady-state boiling conditions. The temperature plot in Fig. 17 reveals that the temperature of the heater remains constant even when the acceleration changes from micro-gravity to $1.8\,g$. The bubble size, however, is gravity-dependent.

It is clearly demonstrated that the heat transfer coefficient is neither influenced by gravity nor by the bubble size at this fluid state. The results are summarized for the wire in the boiling curves at saturated states for various pressures in Fig. 18. The symbols represent the data obtained under micro-gravity, while the lines represent the 1-g-data measured immediately after the low-gravity in the consecutive period of the parabola. The evaluation of the heat transfer coefficient ratio α/α_1 versus heat flux density is shown in Fig. 19. α is the heat transfer coefficient under micro-gravity, α_1 at 1-g. It becomes obvious that the heat transfer coefficient for low heat flux loads, especially for wires, is even higher than in earth-gravity. This may be contributed to the fact that in low-gravity all nuclei sites on the wire are equally activated.

Figure 19:   Dependence of the heat transfer coefficient ratio α/α_1 of various correlations extrapolated to lower and higher accelerations a/g and compared to experimental results.

coefficient may be caused by the smaller surface tension, which is responsible for the departure of the bubbles as discussed later. Several correlations from the literature are evaluated in Fig. 19 with respect to their influence on the acceleration level a/g. Indeed, all these correlations were developed under earth-gravity conditions and are valid for $a/g = 1$ only. However, if the physics of the boiling process were be described correctly, an extrapolation to lower or higher accelerations should be implicitly possible without too large deviations from the experimental findings. The great deviations, however, support the statement given above that the physics of the boiling process is not properly represented in most correlations.
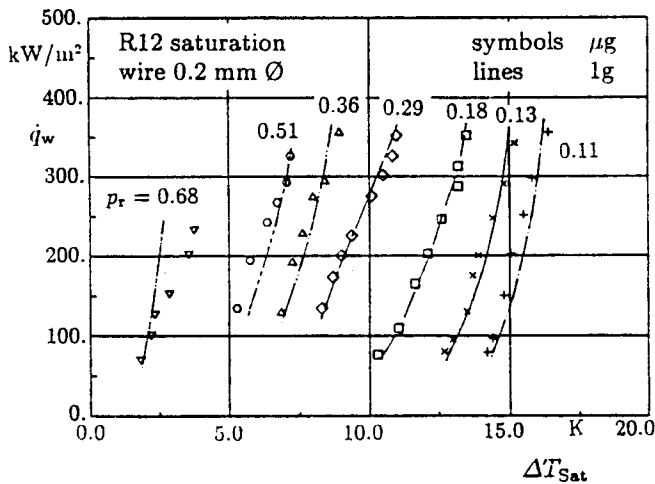

Figure 18:   Nucleate boiling curves for a wire of 0.2 mm diameter in R12 at various saturated fluid states.

As a result, boiling occurs symmetrically around the wire in low-gravity, whereas in 1-g, the lower stagnation point is cooled by free convection, and only the upper circumference of the wire is preferred for boiling. The reduction of the heat transfer coefficient at higher heat fluxes is caused by the higher bubble density and the appearance of larger bubbles due to bubble coalescence connected with the increase of dry areas below the bubbles. For lower pressures $p/p_c < 0.1$, not shown here, the bubbles and the dry areas below them are large due to the small density of the vapor. Therefore, the heat transfer is reduced. At higher system pressures $p/p_c \geq 0.7$, the reduction in the heat transfer
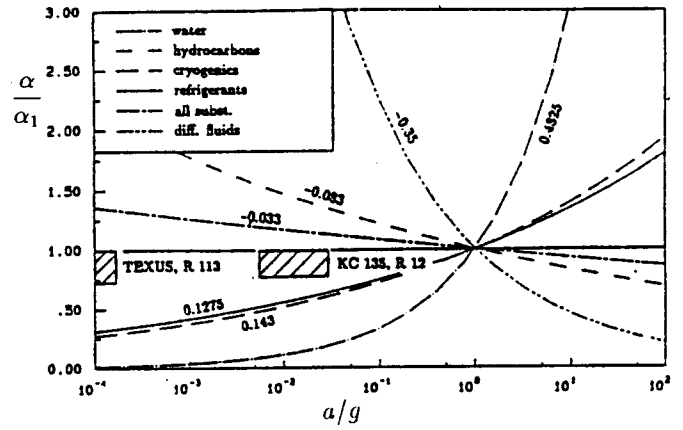
2   Mechanism of Nucleate Boiling

Finally, the question arises, what are the physical mechanisms of nucleate boiling, and how can the transport of energy be explained in the absence of buoyancy. For a better understanding, it is useful to divide the mechanism of the boiling process into a primary and some secondary mechanisms:

- The primary mechanism is the formation and the growth of the bubbles in the superheated liquid boundary layer by evaporation at the liquid-vapor interface. Most important for the heat transfer is the edge at the solid-liquid-vapor interface on the baseline of the bubbles. In this region, the evaporation rate is very high and not influenced by gravity but only by the temperature of the heater.

- The secondary mechanisms are responsible for the heat transport from the heater surface to the bulk liquid. This occurs by the departing bubbles carrying away latent heat, by the wake-flow following the bubbles, and by convection.

In forced convection boiling, the bubbles and the liquid are

carried away by the flow, and in pool boiling under earth-gravity, they are carried away by buoyancy. In micro-gravity, the various effects observed are mostly caused by surface tension, they are shortly summarized:

- inertia forces during rapid growth;

- vertical and horizontal bubble coalescence, followed by the inertia of the liquid lifting the bubbles and supplying cool liquid to the heater;

- coalescence of small bubbles into larger bubbles;

- lifting and replacement of large bubbles by the growth of smaller ones below them.

In subcooled liquids, additional effects are observed:

- pumping by high frequency growth and condensation, called micro-convection, observed with small bubbles on earth;

- in micro-gravity, large bubbles are formed with evaporation at the bubble base and condensation at the crown;

- thermocapillary convection;

- coalescence of small bubbles with large bubbles and condensation at the top. The large bubbles grow into regions, where the liquid is still subcooled. Partial condensation of large bubbles at the top occurs with dynamic fluid motion.

It is interresting to note, that the overall heat transfer coefficient is only less dependent on these secondary mechanisms.

3 Critical Heat Flux

Under micro-gravity, nucleate boiling can be maintained at much higher heat fluxes than expected. Therefore, it is obvious that even the critical heat flux must be shifted to higher values than predicted by the generally accepted hydrodynamic theory of vapor film instability. In Fig. 20, results of wires are plotted in a graph similar to the one originally used by Lienhard and Dhir [25], where the dimensionless radius R' is extended over two decades, and the critical heat flux ratio is on a logarithmic scale. The 900 data points following the extended relation for wires, are sketched as an area, and the 60 data points found in drop-towers not obeying this relation are also marked. The values we obtained on TEXUS and parabolic aircraft flights for wires are about 20 times higher than the predicted values for the flat plate and more than 3 times higher than the extrapolated theory of wires predicts. Even the values obtained on the flat plate in TEXUS are more than 2 times higher than the predicted ones. For practical technical applications under microgravity, these high heat fluxes are very promising to use boiling as an efficient mode of heat transfer.
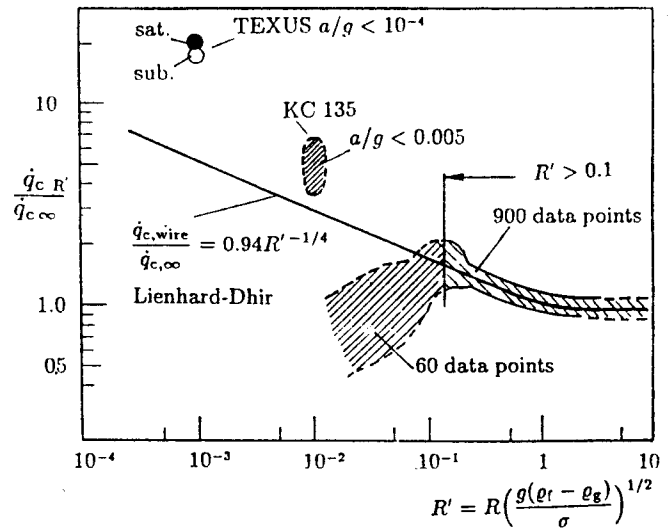

Figure 20: Critical heat flux for wires in an extended plot according to Lienhard and Dhir.

4 Film Boiling

As the measured film boiling data on wires indicate in Fig. 21, the correlations of Pitschmann [26], Bromley [27] and Frederking and Clark [28] can obviously be extrapolated at least to $a/g = 10^{-2}$. These relations are developed on the concept of Nusselt's film theory and thus they describe the physical mechanisms better than the nucleate boiling correlations. Film boiling is maintained by a mechanism caused by surface tension. A chain of large and small bubbles is formed around the wire (Fig. 22), and vapor is pumped from the smaller bubbles into the larger ones due to the higher pressure in the smaller bubbles. The vapor is pumped by contracting and expanding of the smaller bubbles in a mode of peristaltic motion.
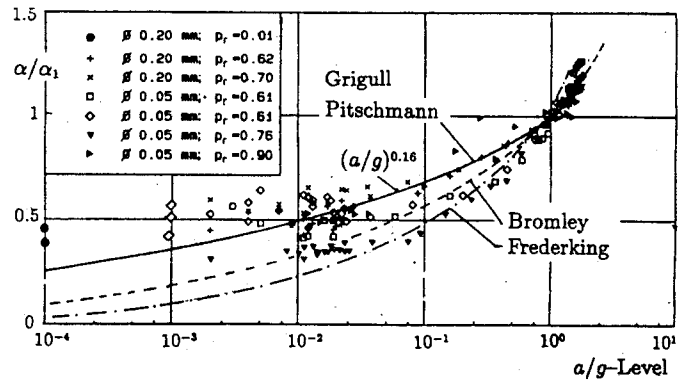

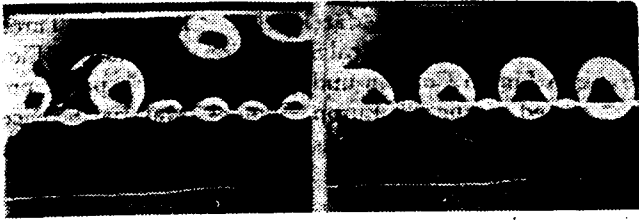Figure 21: Film boiling data with corresponding correlations.

26

Figure 22: Film boiling on a wire under micro-gravity.

Summary

In this paper, the most important transport phenomena for heat and mass transfer in micro-gravity are discussed. The excitation of convection by acceleration pulses during materials processing is certainly an undesirable effect, but it is also a transport process, which can only be simulated numerically. In order to study the effect at the solidification front itself, the diffusion process in the material must be considered, too. However, from this investigation general statements and recommendations can be drawn. For very sensitive experiments, special 3-dimensional calculations have to be performed, where all parameters of influence are considered.

Thermocapillary flow is much more important for heat transport than it was estimated before. The enhancement of heat transfer is remarkable, however, at higher Marangoni numbers the influence is weakened, because the strong flow at the interface itself reduces the driving temperature gradients. Therefore, oscillatory flow occurs in a rectangular cavity with a bubble in the center of the liquid. In a liquid column, even at very high Ma numbers no oscillation could be observed in the 3-dimensional simulation, which is contradictory to other authors.

Boiling, as the most efficient heat transfer mechanism, can be maintained in micro-gravity. Buoyancy does not play the role it has been attributed to until now, nearly the same heat transfer values as on earth are observed in microgravity. The dominating effect for boiling is evaporation at the edge of the interface solid-liquid-vapor. The energy transport from the heater surface to the bulk liquid is governed by mechanisms in which surface tension is involved, such as bubble coalescence, liquid inertia, and replacement of bubbles. In subcooled liquids, evaporation at the base, and condensation at the top of the bubble induce a highly dynamic liquid motion, and transport cooler liquid to the heater surface. Film boiling can be stabilized under microgravity with surface tension forming a chain of large and small bubbles pumping the vapor by peristaltic motion to the larger bubbles.

We did not discuss condensation heat transfer in microgravity. It seems that the basic mechanisms are the same as on earth. However, attention has been given to the liquid transport from the condensation surface which can be attained by a special capillary structure on the surface. Here

as well, the surface tension is the driving mechanism for the transport of liquid.

We can conclude: Surface tension together with its related processes is the most important quantity and force for heat and mass transfer phenomena in micro-gravity. It can replace totaly or partly the role of buoyancy. Micro-gravity is a useful environment to study transport phenomena without buoyancy in more detail for a better understanding of the physics behind them.

Acknowledgement

References

[1] Schneider, S., Heiss, T., and Straub, J., "Natural Convection in a Cylinder caused by Gravitational Interferences: A Three-Dimensional Numerical Calculation", *Proc. Intern. Symp. on Thermal Problems in Space-Based Systems*, ASME HTD 83, Dobran, F., Imber, M. (eds.), New York, ASME, pp. 77-83 (1987).

[2] Schneider, S., and Straub, J., "Influence of the Prandtl Number on Laminar Natural Convection in a Cylinder caused by g-Jitter", *J. Crystal Growth*, Vol. 97, pp. 235-242 (1989).

[3] Schneider, S., "Laminare freie Konvektion in einem Zylinder bei konstanter und zeitveraenderlicher Schwerkraft (g-jitter)", doctoral thesis, Technical University of Munich (1990).

[4] Straub, J. and Schneider, S., "Transient Convection caused by Acceleration Disturbances", *Microgravity Sci. Technol.*, Vol. 5, No. 1, pp. 27-34 (1992).

[5] Schneider, S. and Straub, J., "Laminar Natural Convection in a Cylindrical Enclosure with Different End Temperatures", *Int. J. Heat Mass Transfer*, Vol. 35, pp. 545-557 (1992).

[6] Straub, J., Weinzierl, A., and Zell, M., "Thermokapillare Grenzflaechenkonvektion an Gasblasen in einem Temperaturgradientenfeld", *Waerme- und Stoffuebertragung*, Vol. 25, pp. 281-288 (1990).

[7] Straub, J., Betz, J., and Marek, R., "Numerical Simulation of Marangoni Convection around Gas Bubbles in a Liquid Matrix", submitted to *Numerical Heat Transfer, pt. A: Applications* (1991).

[8] Straub, J., Betz, J., and Marek, R., "Numerical Simulation of Marangoni Convection around Gas Bubbles in a Liquid Matrix", paper presented at the 8th Europ. Sympos. Material Sciences in Microgravity, Brussels, Belgium, to be published as ESA-SP 333 (1992).

[9] Chun, Ch.H. and Wuest, W., "Experiments on the Transition from the Steady to the Oscillatory Marangoni-Convection of a Floating Zone under Reduced Gravity", *Acta astronautica*, Vol. 6, No. 9, pp. 1073-1082 (1979).

[10] Preisser, F., Schwabe, D., and Scharmann, A., "Steady and Oscillatory Thermocapillary Convection in Liquid Columns with Free Cylindrical Surface", *J. Fluid Mech.*, Vol. 126, pp. 545-567 (1983).

[11] Rupp, R., Mueller, G., and Neumann, G., "Three-Dimensional Time Dependent Modelling of the Marangoni Convection in Zone Melting Configurations for GaAs", *J. Crystal Growth*, Vol. 97, pp. 34-41 (1989).

[12] Schwabe, D. and Scharmann, A., "Some Evidence for the Existence of a Critical Marangoni Number for the Onset of Oscillatory Flow in Crystal Growth Melts", *J. Crystal Growth*, Vol. 46, pp. 125-131 (1979).

[13] Schwabe, D., Preisser, F., and Scharmann, A., "Verification of the Oscillatory State of Thermocapillary Convection in a Floating Zone under Low Gravity", *Acta astronautica*, Vol. 9, No. 4, pp. 265-273 (1982).

[14] Schwabe, D., Velten, R., and Scharmann, A., "The Instability of Surface Tension Driven Flow in Models for Floating Zones under Normal and Reduced Gravity", *J. Crystal Growth*, Vol. 99, pp. 1258-1264 (1990).

[15] Chun, Ch.H., "Marangoni Convection in a Floating Zone under Reduced Gravity", *J. Crystal Growth*, Vol. 48, pp. 600-610 (1980)

[16] Monti, R., Napolitano, L.G., and Mannara, G., "Texus Flight Results on Convective Flows and Heat Transfer in Simulated Floating Zones", Proc. 5th Europ. Sympos. Material Sciences under Microgravity Conditions, Schloss Elmau, ESA SP-222, pp. 229-236 (1984).

[17] Kamotani, Y., Ostrach, S., and Vargas, M., "Oscillatory Thermocapillary Convection in a Simulated Floating-Zone Configuration", *J. Crystal Growth*, Vol. 66, pp. 83-90 (1984).

[18] Marek, R. and Straub, J., "Three-Dimensional Transient Simulation of Marangoni Flow in a Cylindrical Enclosure under Various Gravity Levels", IUTAM Symposium on Microgravity Fluid Mechanics, Bremen, Germany. (An extended abstract of this study has been published in: *Microgravity Science and Technology*, Vol. 4, No. 2, pp. 153-154 (1991)

[19] Straub, J. and Marek, R., "Transient Three-Dimensional Numerical Simulation of Marangoni Flow in a Liquid Column under Microgravity", paper presented at the 8th Europ. Sympos. Material Sciences in Microgravity, Brussels, Belgium, to be published as ESA-SP 333 (1992).

[20] Dhir, V.K., "Nucleate and Transition Boiling Heat Transfer under Pool Boiling and External Flow Conditions.", Proc. 9th International Heat Transfer Conference, Jerusalem, Israel, Vol. 1, pp. 129-155, (1990).

[21] Straub, J., Zell, M., and Vogel, B., "Pool Boiling in a Reduced Gravity Field", Proc. 9th International Heat Transfer Conference, Jerusalem, Israel, Vol. 1, pp. 91-112 (1990).

[22] Zell, M., Straub, J., and Vogel, B., "Pool Boiling under Microgravity", *J. of Physico-Chemical Hydrodynamics*, Vol. 11, Nos. 5/6, pp. 813-823 (1989).

[23] Straub, J., Zell, M., and Vogel, B., "Boiling under Microgravity Conditions", paper presented at the 1st Europ. Sympos. Fluids in Space, Ajaccio, France, 1991, to be published by ESA (1992).

[24] Zell, M., "Untersuchung des Siedevorgangs unter reduzierter Schwerkraft", doctoral thesis, Technical University of Munich (1991).

[25] Lienhard, J.H. and Dhir, V.K., "Extended Hydrodynamic Theory of the Peak and Minimum Pool Boiling Heat Fluxes", NASA CR 2270 (1973).

[26] Pitschmann, P. and Grigull, U., "Film Boiling on Horizontal Cylinders", *Waerme- und Stoffuebertragung*, Vol. 3, pp. 75-84 (1970).

[27] Bromley, L.A., "Heat Transfer in Stable Film Boiling", *Chem. Eng. Prog.*, Vol. 46, pp. 221-227 (1950).

[28] Frederking, T.H.K. and Clark, J.A., "Natural Convection Film Boiling on a Sphere", *Adv. Cryogen. Eng.*, Vol. 8, p. 501 (1963).

For additional literature, we refer to the reference list in the cited articles.